Materials Science Forum
ISSN: 1662-9752, Vol. 1185, pp 19-28
doi:10.4028/p-aok1H1

Submitted: 2025-12-21
Revised: 2026-02-13
Accepted: 2026-02-23
Online: 2026-04-15

Influence of Tumbling-Induced Geometric Anisotropy on the Mechanical Performance of Self-Piercing Rivet Joints

Jessica Sarris[1,a*], Michael Lechner[1,b]

[1]Institute of Manufacturing Technology, Friedrich-Alexander-Universität Erlangen-Nürnberg, Egerlandstr. 13, 91058 Erlangen, Germany

[a]jessica.sarris@fau.de, [b]michael.lechner@fau.de

Keywords: Self-Piercing Riveting (SPR), Versatile Joining, Asymmetric Tumbling, Tumbling Self-Piercing Riveting (T-SPR)

Abstract. Conventional self-piercing riveting (SPR) produces rotationally symmetric joints with largely uniform mechanical behavior. While this provides robust performance in many applications, increasing demands for material-efficient lightweight design, complex load paths and hybrid material systems require more versatile joining strategies. Recent experiments have demonstrated that an adapted tumbling SPR (T-SPR) process can intentionally induce non-rotationally symmetric joint geometries and thereby extend process limits beyond those of conventional SPR. Such asymmetric joints offer the potential to tailor load-bearing capacity and energy absorption to specific load directions, which could be particularly advantageous in crash-relevant or multi-material applications. Building on these findings, the present study shifts the focus from geometry control to the systematic evaluation of the mechanical performance of asymmetric T-SPR joints. Specimens were produced using T-SPR with tailored combinations of tumbling angle and velocity. The joints are manufactured with a versatile tumbling self-piercing riveting tool. To assess the resulting mechanical properties, cross tensile and tensile shear tests are conducted. From the resulting force-displacement curves, typical mechanical properties such as ultimate load, load-bearing capacity, displacement at failure and absorbed energy are derived. The mechanical performance of asymmetric joints is evaluated in comparison with symmetric reference joints produced by tumbling self-piercing riveting. This enables both the demonstration of direction-dependent mechanical behavior of asymmetric joints compared to symmetric references and a systematic evaluation of how geometric anisotropy affects load-bearing capacity, absorbed energy and failure characteristics.

Introduction

Lightweight design is one of the key elements for achieving the targets of reducing CO_2 emissions over the entire vehicle life cycle [1]. In this context, application-specific material design is of central importance [2]. The industrial implementation of such lightweight structures requires joining technologies that are capable of connecting materials with high process reliability and without thermal influence on the microstructure [3]. Mechanical joining, in particular SPR, has become established as the dominant technology in the automotive industry [4]. In addition to the high process forces required and the need for a rigid machine setup [5], the rigid and purely axial punch kinematics produce rotationally symmetric joints. SPR therefore generates direction-independent joint properties, although body-in-white structures are often subjected to complex, anisotropic load paths, for which a directionally tailored adaptation of joint properties would be advantageous. This is why adaptable joining processes are required. One approach extending the process limits is tumbling self-piercing riveting (see Fig. 1). T-SPR is an incremental further development of the conventional SPR, in which the completely translational axial motion of the punch is superimposed by a tumbling kinematics [6]. In contrast to conventional self-piercing riveting, the punch in T-SPR has a conical shape and therefore does not act on the rivet over its entire contact area [7].

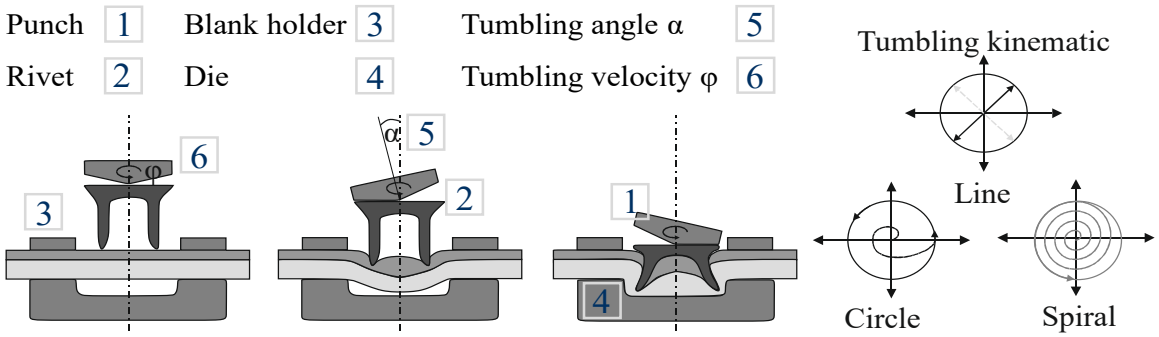

Fig. 1. Tumbling self-piercing riveting (T-SPR) process and tumbling kinematics

The conical tumbling punch performs a rolling motion on the rivet head, and the resulting reduced contact area leads to lower maximum process forces [8]. In contrast to SPR, the forming force is not introduced globally but is concentrated locally [9]. The individual process steps of T-SPR, namely clamping, piercing, spreading and setting, are identical to those of conventional self-piercing riveting [10], with the exception of the tumbling punch. In this study, the load-bearing capacities and fracture behavior of asymmetrically tumbled self-piercing riveted joints are investigated in comparison with symmetrically tumbled reference joints with two identical joining partners.

Experimental Test Setup

The material used in this study is a precipitation-hardenable aluminum alloy of the 6xxx series on an Al-Mg-Si basis, EN AW-6014 in the T4 temper, with an initial sheet thickness of $t_0 = 2.0$ mm on the die side and a sheet thickness of $t_0 = 1.0$ mm on the punch side. The alloy has been developed for automotive outer panel applications and is characterized by a high forming capability [11].

Joining by tumbling self-piercing riveting (T-SPR). The joining experiments have been realized on a universal testing machine (type Walter + Bai FS-300) equipped with an integrated versatile tumbling tool (see Fig. 2) [6], which simultaneously records the force-displacement curves. By integrating the versatile tool into the universal testing machine, the punch stroke is directly applied via the machine's crosshead movement in the z-direction. The tumbling motion is generated by a two-axis drive mechanism consisting of a linear and a rotary actuator. The kinematic coupling of the two axes enables controlled positioning at any point on the circular path and thus freely programmable tumbling strategies.

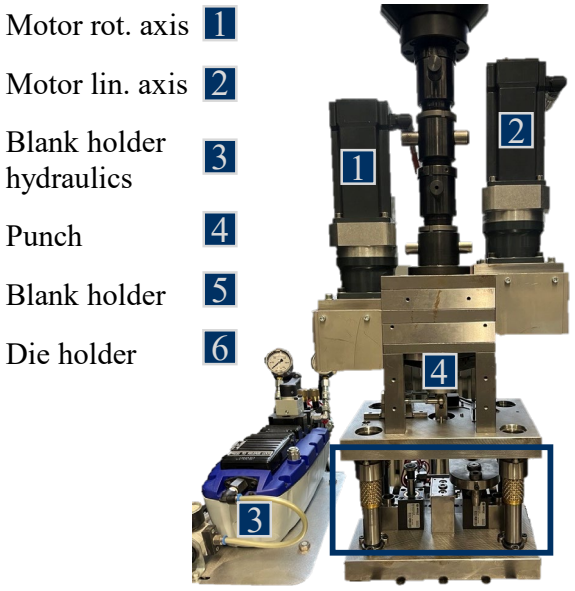

Tool parameters	
$F_{max,\ punch}$	100 kN
α_{max}	7°
Punch kinematic	Versatile

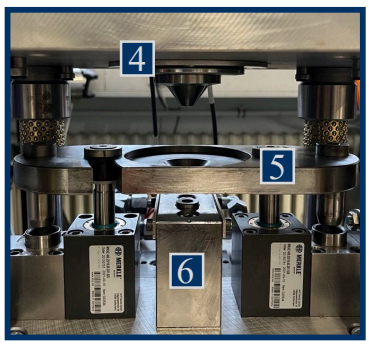

Fig. 2. Tumbling self-piercing riveting tool and tool specifications

Within the scope of this study, both symmetric and asymmetric tumbling strategies are considered. For the symmetric strategies, tumbling angles of $\alpha = 1°$ and $\alpha = 5°$ are investigated. In the symmetric 1° strategy, the punch is moved around the tool axis at a constant tumbling angle of $\alpha = 1°$ starting from the tumbling onset h_{t0}. The angle remains constant over the entire tumbling phase and is reduced to zero during one final tumbling revolution. The symmetric 5° strategy is implemented equally. The asymmetric 1°/5° strategy is defined such that, within one full revolution of the tumbling punch, 180° of the rivet circumference are tumbled with $\alpha = 1°$ and the remaining 180° with $\alpha = 5°$. This angle profile is repeated continuously until the end of the tumbling process. The onset of tumbling is chosen such that the rivet has fully pierced the upper sheet layer before the tumbling motion is activated, in order to prevent rivet tilting. Tumbling velocities of $\varphi = 90°/s$, 180°/s and 360°/s are investigated. The crosshead velocity v_t is adjusted in each case to keep the stroke per revolution constant, thereby changing only the temporal sequence of the local forming steps and, consequently, the local forming speed. This makes it possible to separate the influence of tumbling velocity from geometric effects. The tool is equipped with a blank holder, which clamps the sheets against the die during joining and thus prevents bulging or lateral displacement of the sheets. The process parameters are summarized in Table 1. For each parameter combination, n = 3 repetitions are carried out.

Table 1. Parameters of the investigation

Die	Rivet	Tumbling angle α [°]	Tumbling onset h_{t0} [mm]	Tumbling velocity φ [°/s]	Tumbling kinematic
FM 090 2016	C5.3x5.0 H4	1/5, 1, 5	2.5	90, 180, 360	Circle

Testing of Load-Bearing Capacity

To investigate the load-bearing capacity of the asymmetrically tumbled self-piercing riveted joints, mechanical tensile shear and cross tension tests are carried out on the specimens. The tests are performed on a ZwickRoell Z10 universal testing machine with a maximum force of 10 kN under quasi-static loading in accordance with [12]. All tests are conducted at a constant crosshead velocity $v_t = 10$ mm/min.

Tensile shear tests. To investigate the load-bearing capacity of the joined connections, the tensile shear strength of specimens with dimensions of 45 x 105 mm² is determined. The focus of this investigation is on the orientation of the asymmetry. Therefore, three different orientations of the maximum tilting (1° side) are considered (Fig. 3). The different orientations of the tilting are defined as follows: (a) maximum tilting oriented towards the 2.0 mm lower sheet, (b) maximum tilting oriented towards the 1.0 mm upper sheet, and (c) maximum tilting located on the left-hand side of the loading direction.

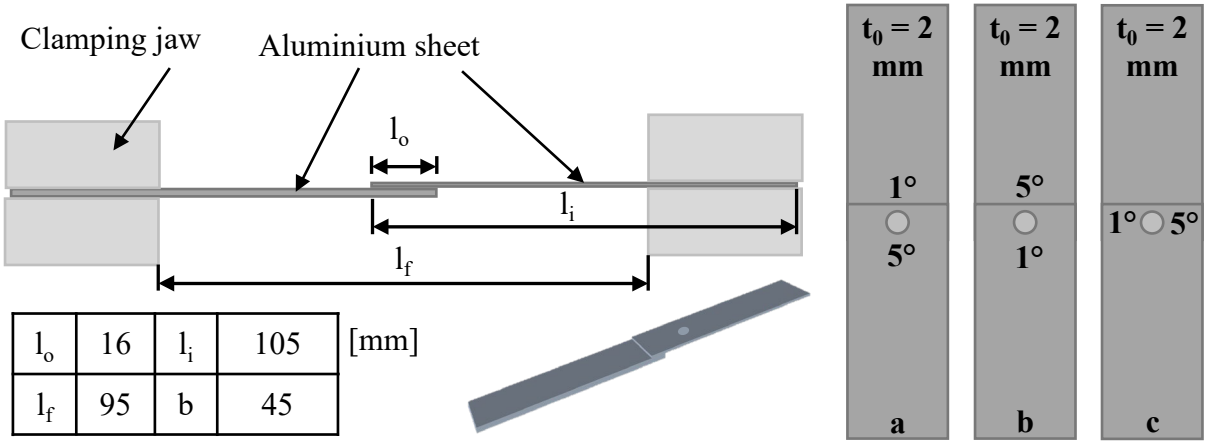

Fig. 3. Illustration of the tensile shear test and the orientations (a), (b) and (c)

The joining partners are joined with an overlap length of 16 mm. The specimen is clamped in the two grips of the universal testing machine with a constant clamping force (Fig. 3). The free clamping

length is 95 mm, according to [12]. During the tests, force and displacement are recorded. In addition, the tensile shear tests are monitored using the Aramis (GOM) digital image correlation system in order to capture displacement and strain fields on the specimen surface, to determine local strains and to analyze the failure behavior. For this purpose, the punch-side surfaces in and around the overlap region are coated with a high-contrast speckle pattern.

Cross tension tests. In addition to the tensile shear tests, cross tension tests are carried out. For this purpose, specimens according to DVS/EFB 3480-1 [12] with dimensions of 50 x 150 mm^2 are used (Fig. 4). The riveted joint is positioned centrally within the overlap of the sheets. The joined specimens are clamped in two specimen holders that are fixed to the upper and lower fixtures of the universal testing machine. During the test, the force and displacement data are recorded by the testing machine. Two orientations of the tilting (1° side) were investigated: in the first case (a), the tilting is aligned with the longitudinal direction of the 1 mm upper sheet, corresponding to a rotation around an axis parallel to the sheet width l_w, whereas in the second case (b) the tilting is rotated by 90° relative to this configuration and is thus aligned with the sheet width l_w, corresponding to a rotation around an axis parallel to the sheet length l.

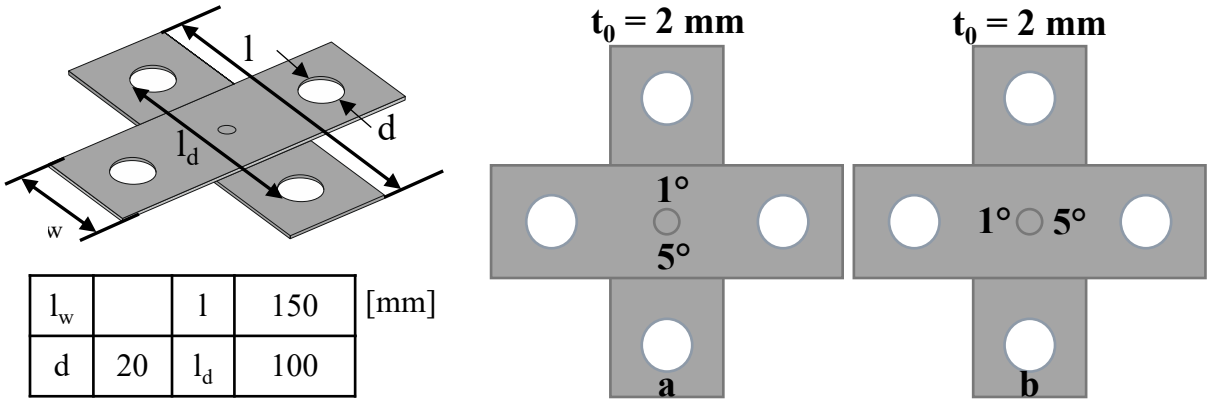

l_w		l	150	[mm]
d	20	l_d	100	

Fig. 4. Illustration of the cross tension test and the orientations (a) and (b)

Results and Discussion

Tensile shear tests. The tensile shear tests are used to evaluate the joint strength of the specimens. To quantify the influence of the process parameters and the geometrical anisotropy, the mean maximum tensile shear forces ($\bar{F}_{max}$) a) are evaluated. In addition to the maximum force, the energy absorption b) of the joint is a decisive indicator of the failure behavior. As an evaluation criterion, the dissipated work up to a decrease of the tensile shear force to 30 % of its maximum value ($W_{0,3F_{max}}$) is considered [12]. Fig. 5 shows the mechanical characteristics as a function of tumbling velocity, orientation of the maximum tilting and the symmetric and asymmetric tumbling strategies.

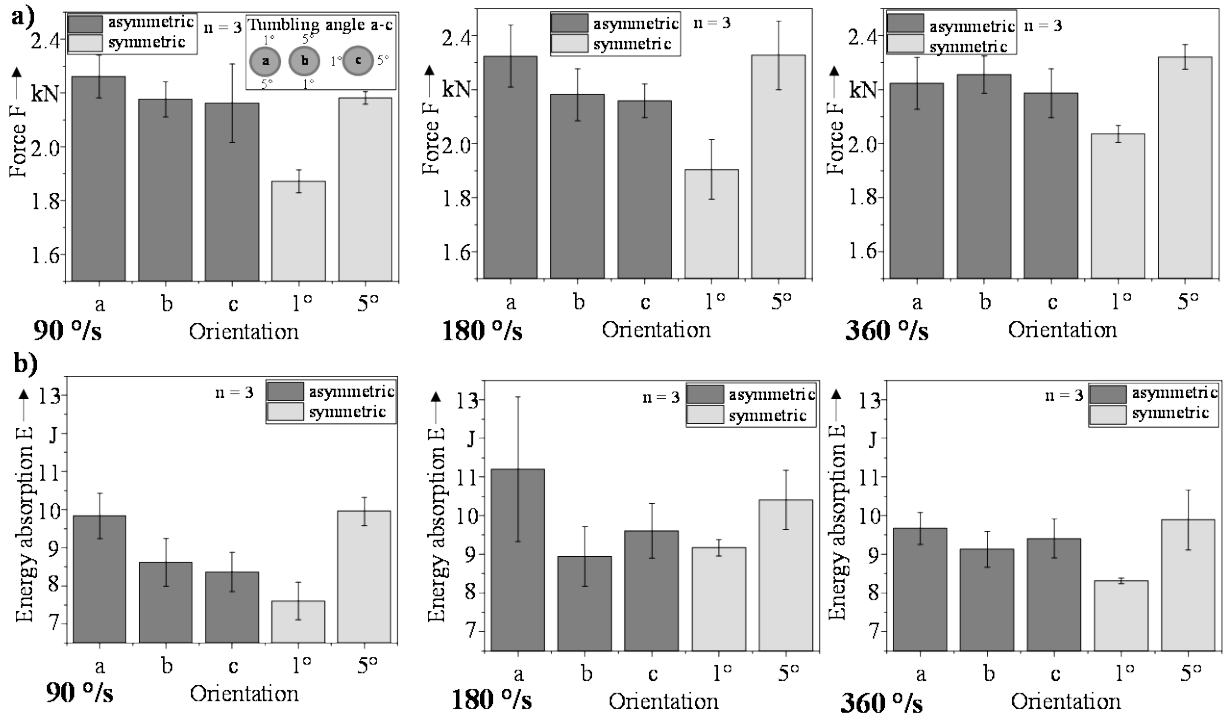

Fig. 5. Mean maximum tensile shear forces and work of specimens for the different tumbling velocities and strategies (symmetric and asymmetric) as a function of orientations (a), (b) and (c)

The symmetric 1° reference specimens reach mean tensile shear forces between approximately 1.9 and 2.03 kN, whereas the symmetric 5° specimens reach clearly higher values of about 2.2 - 2.3 kN, when considering the forces across all investigated tumbling velocities. Thus, a larger tumbling angle increases the tensile shear load-bearing capacity by around 18 %. In comparison, the influence of the tumbling velocity φ is small. The average increase in force of about 17.5 % confirms that the larger tumbling angle of $\alpha = 5°$ generates a more noticeable undercut due to stronger radial material displacement, which provides a higher resistance against tensile shear loading. The 1° reference group exhibits the lowest energy absorption capacity with approximately 7.6 - 9.2 J, whereas the 5° specimens reach significantly higher values of about 10 J. This correlates with the more pronounced undercut of the 5° joints.

For the asymmetrically tumbled joints ($\alpha = 1°/5°$), tensile shear forces between 2.15 kN and 2.32 kN and dissipated energies up to 11.2 J are achieved. On average, these values lie slightly above the symmetric references ($\bar{F}_{max,\,symm} = 2.14$ kN), representing the combined mean of the symmetric 1° and 5° reference specimens. In particular, orientation (a) (maximum tilting towards the 2 mm lower sheet) reaches or even exceeds the level of the symmetric 5° references, which indicates an undercut that is more effective in the shear direction. As shown in previous investigations, the undercut on the 1° tumbled side is more pronounced than on the 5° side. The larger angle in the 5° sector results in higher local contact pressure and a stronger geometric deformation of the rivet head by the punch [13]. Due to the larger contact area, the opposite 1° sector is subjected to lower local forming pressure. As a consequence, the rivet and sheet material displaced on the 5° side may flow into the 1° sector, causing the rivet foot to flare more strongly in the radial direction and thereby increasing the undercut. A dependence of the shear strengths on the loading rates for the asymmetric specimens is hardly noticeable. It can be seen that orientation (a) reaches the highest force at $\varphi = 180$ °/s, whereas (b) and (c) show similar values across the three velocities. For the symmetric specimens, a stronger dependence on the velocities is observed. As φ increases, both the forces and work increase.

Failure behavior in tensile shear tests. In the following, the failure behavior of the individual orientation groups (a), (b) and (c) is analyzed. Fig. 6 shows the tensile shear forces of the different

orientation groups. All joints were produced using the asymmetric tumbling strategy with a tumbling angle of α = 1°/5° and a tumbling velocity of φ = 180 °/s.

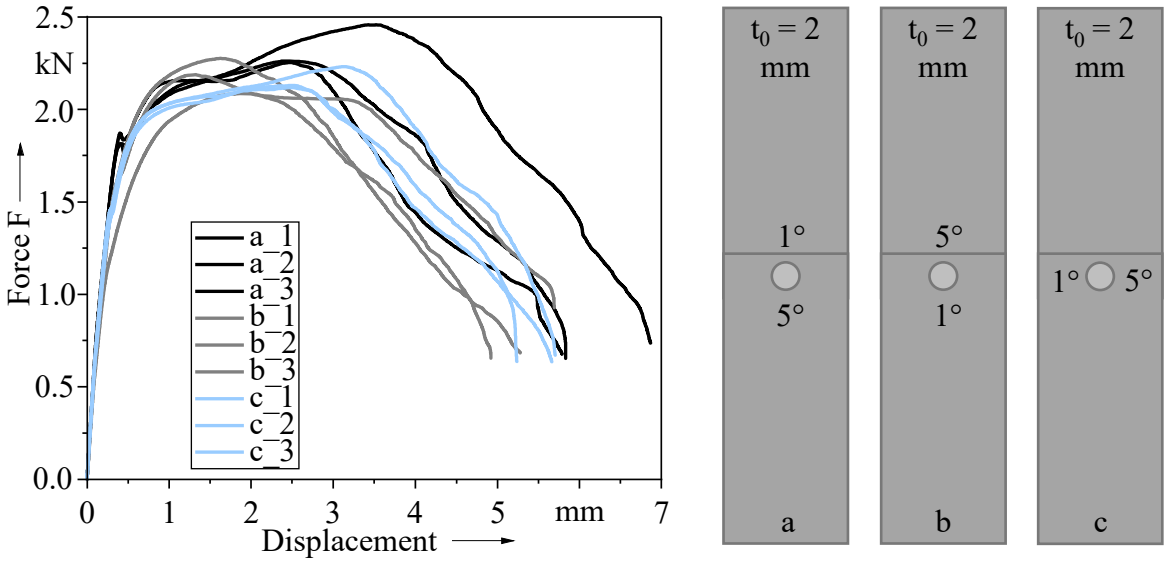

Fig. 6. Force-displacement curves of the asymmetrically tumbled joints for the three orientations (a), (b) and (c) under tensile shear forces

At the beginning of the test, the force increases similarly for all specimens up to a displacement of approximately x = 0.5 mm. Subsequently, the force-displacement curves diverge depending on the orientation of the maximum tilting. Notably is specimen a_3, which exhibits the highest tensile shear maximum and the largest displacement. For interpretation, the major and minor strains as well as the tensile strains in loading direction εy are analyzed for the three orientations at displacements of x = 1.0 - 4.0 mm and a tumbling velocity of φ = 180 °/s (Fig. 7, Fig. 8 and Fig. 9).

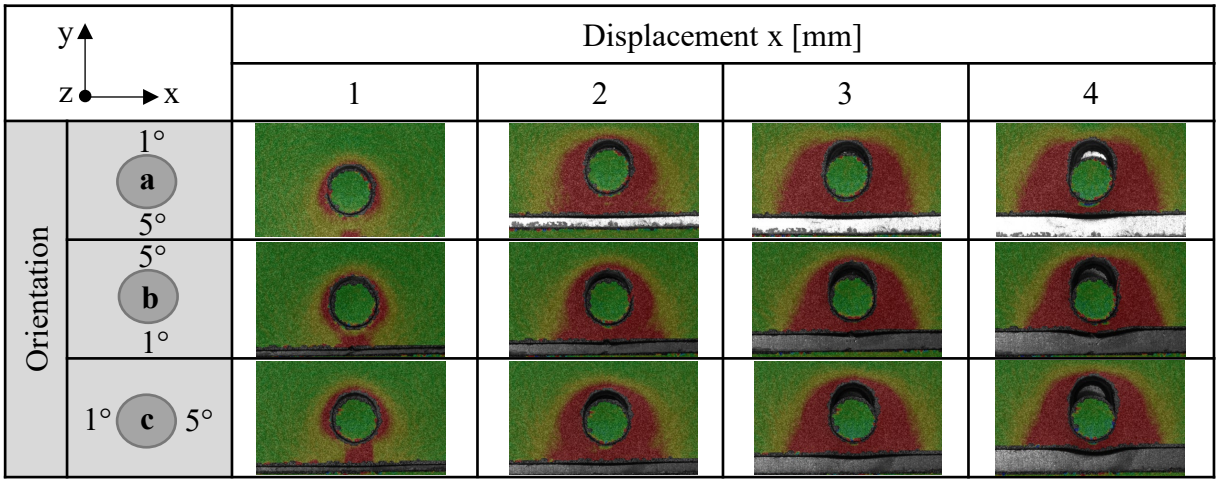

Fig. 7. Comparison of major strains for orientations (a), (b) and (c)

Fig. 7 shows the evolution of the major strain fields for orientations (a), (b) and (c). For orientation (a), the major strains localize in a narrow band below the rivet along the shear path, which is consistent with the highest tensile shear force and energy absorption. In contrast, orientations (b) and (c) exhibit more distributed and partly laterally shifted major strain zones, indicating a less efficient utilization of the local deformation capacity in the main load path.

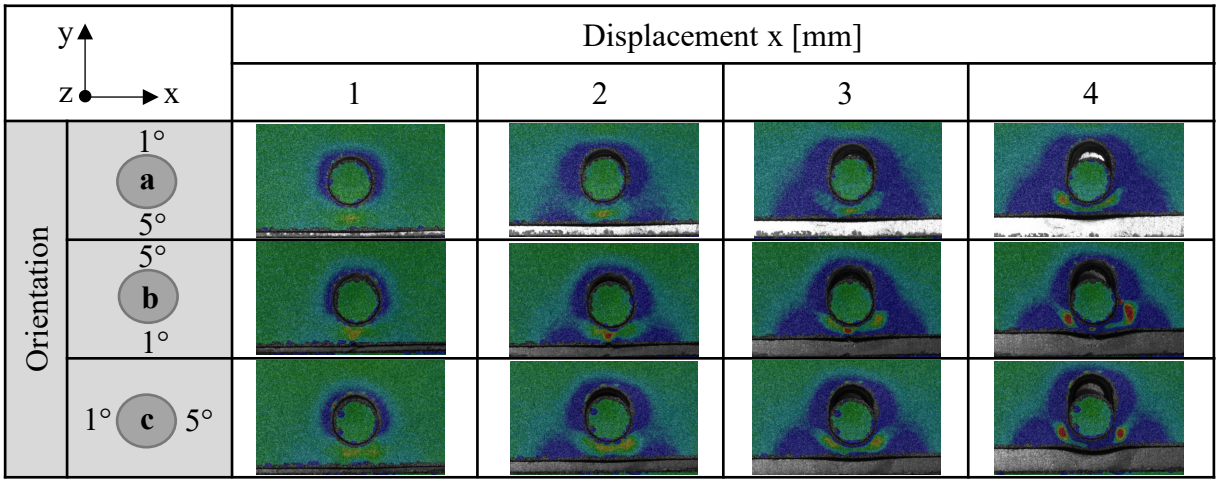

Fig. 8. Comparison of minor strains for orientations (a), (b) and (c)

Fig. 8 illustrates the corresponding minor strain fields. When looking at the strains, a continuous expansion of the blue compressive zone can be observed between 1 and 3 mm. This is attributed to the material increasingly contracting in the rivet region to compensate for the longitudinal strain. At 4 mm displacement, interruptions of the compressive zone appear for (b) and (c) in the form of compression (red). Orientation (a) exhibits a more ductile and stable response, with a smooth transverse contraction up to failure. In contrast (b) and (c) show a more unstable end-stage behavior, characterized by localized minor-strain hotspots at x = 4 mm, indicating pronounced, highly concentrated constriction or shear deformation that is not observed for orientation (a).

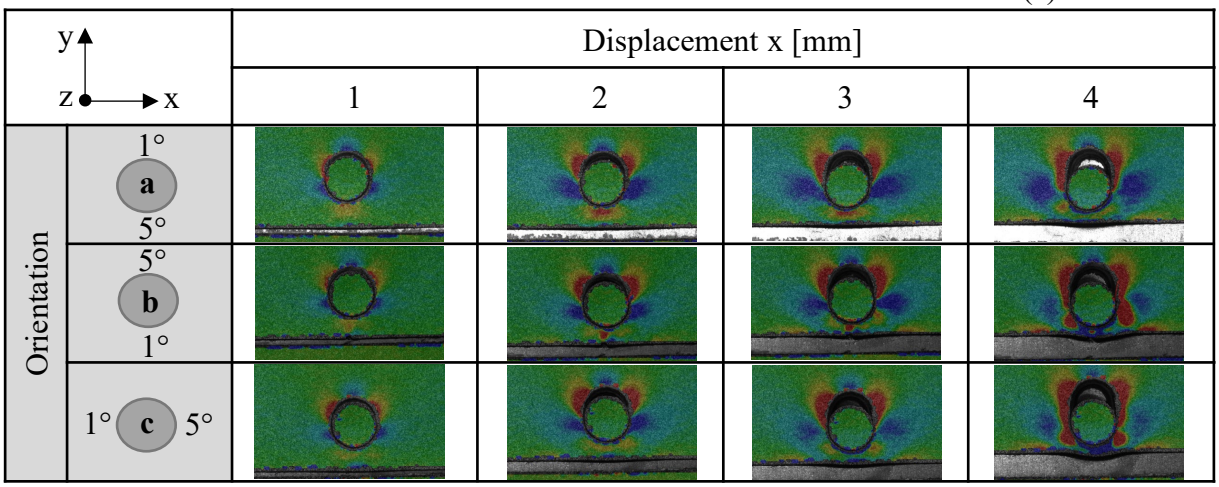

Fig. 9. Comparison of strains in y-direction (loading direction) for orientations (a), (b) and (c)

Fig. 9 compares the strains in y-direction (loading direction) for the three orientations. Orientation (a) is characterized by smaller regions of tensile strain (red) and more extensive compressive zones (blue) compared to orientations (b) and (c). At x = 4 mm, orientation (a) shows a more diffuse and slightly wider distribution of tensile strains (red). In contrast, for orientations (b) and (c), the red regions are more pronounced and concentrated around the rivet, indicating a different deformation behavior compared to (a). One possible reason is the arrangement of the tumbling angles, which leads to a direction-dependent load path in the rib. Depending on the orientation, the tensile forces are either distributed over a wider area (orientation (a)) or introduced more locally into the material (orientations (b) and (c)). This interpretation is consistent with the tensile shear results in Fig. 5, where orientation (a) exhibits the highest tensile shear forces.

Cross tension tests. Fig. 10 shows the mean maximum cross tension forces a) and the dissipated work b) up to a decrease of the cross tension force to 30 % of its maximum value ($W_{0,3F_{max}}$) [12] as

a function of tumbling velocity, tumbling strategy (symmetric/asymmetric) and orientation of the maximum rivet tilting (a) and (b).

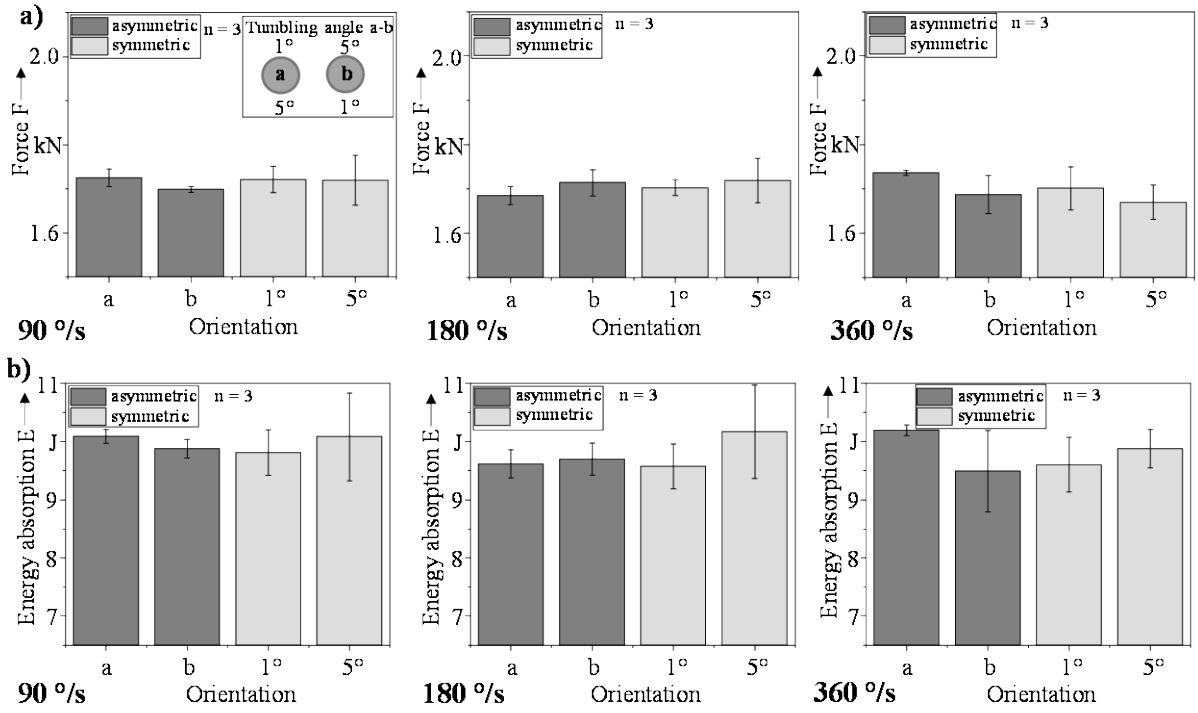

Fig. 10. Mean maximum cross tension forces and dissipated work of the specimens for the different tumbling velocities and tumbling strategies (symmetric and asymmetric) as a function of orientations (a), (b) and (c)

The cross tension parameters indicate an overall robust process behavior. The mean maximum cross tension forces for all investigated parameter combinations lie within a narrow range of approximately 1.67 - 1.74 kN. Neither the tumbling strategy (symmetric vs. asymmetric) nor the tumbling angle or tumbling velocity exhibits a pronounced influence. The work is about 10 J for all groups, with the 5° references reaching only slightly higher values than the 1° specimens. The asymmetrically tumbled joints thus achieve, in cross tension, the same level as the symmetric references and tend to exhibit slightly lower scatter.

Failure behavior in cross tension tests. The failure patterns of all specimens are very similar. In all tests, the rivet remains in the matrix-side lower sheet (t_0 = 2.0 mm), while the punch-side upper sheet is pulled out of the rivet interlock (cross tension failure by sheet pull-out). No systematic differences in failure behavior could be identified between the symmetrically and asymmetrically tumbled joints.

Summary and Outlook

This study investigates the load-bearing capacities of asymmetrically tumbled self-piercing riveted joints produced by a tumbling self-piercing riveting process in aluminum-aluminum (EN AW-6014 T4) sheet combinations with a die-side sheet thickness of t_0 = 2.0 mm and a punch-side sheet thickness of t_0 = 1.0 mm. Tensile shear tests, including digital image correlation using Aramis (GOM), as well as cross tension tests were carried out in order to evaluate the load-bearing capacities of the asymmetric riveted joints in comparison with symmetric reference joints. In addition, the failure behavior was analyzed.

The key findings can be summarized as follows:

1. The asymmetric tumbling strategy (α = 1°/5°) enables a targeted adjustment of anisotropic strength properties.
2. The asymmetric joints do not reach the mean value of the symmetric references but reach the tensile shear load-bearing level of the 5° reference and exceed the 1° reference values.

3. Orientation (a) (maximum tilting orientated towards the 2 mm lower sheet) uses the geometric effects most efficiently.
4. The cross tension tests demonstrate a remarkable process robustness.
5. The joint can be orientated such that the maximum tensile shear strength is aligned with the principal load direction without compromising the axial load-bearing capacity in cross tension.

Due to the extensive use of multi-material systems, future investigations should be extended to multi-material joints, such as aluminum-steel, where stronger forming effects and a more pronounced geometric anisotropy are expected.
In addition to fully asymmetric tumbling strategies, hybrid process concepts combining an initial asymmetric tumbling phase with a subsequent symmetric tumbling phase could be promising. While the asymmetric phase can create a direction-dependent undercut tailored to the dominant load path, the symmetric step may help to homogenize the joint geometry and reduce local stress peaks. Such a hybrid structure could offer improved load-bearing capacities and should be investigated in future studies.

Acknowledgement

Funded by the Deutsche Forschungsgemeinschaft (DFG, German Research Foundation) – TRR 285/2 – Project-ID 418701707. The authors thank the German Research Foundation for their organisational and financial support. Data regarding the contents of the publication can be requested at www.trr285.de.

References

[1] G. S. Cole and A. M. Sherman, "Light weight materials for automotive applications," Materials Characterization, vol. 35, no. 1, pp. 3–9, 1995, doi: 10.1016/1044-5803(95)00063-1.

[2] P. K. Mallick, Materials, Design and Manufacturing for Lightweight Vehicles. Woodhead Publishing, 2020.

[3] H. Q. Ang, "An Overview of Self-piercing Riveting Process with Focus on Joint Failures, Corrosion Issues and Optimisation Techniques," Chin. J. Mech. Eng., vol. 34, no. 1, 2021, doi: 10.1186/s10033-020-00526-3.

[4] D. Li, A. Chrysanthou, I. Patel, and G. Williams, "Self-piercing riveting-a review," Int J Adv Manuf Technol, vol. 92, 5-8, pp. 1777–1824, 2017, doi: 10.1007/s00170-017-0156-x.

[5] M. Merklein, M. Jäckisch, C.-M. Kuball, D. Römisch, S. Wiesenmayer, and S. Wituschek, "Mechanical joining of high-strength multi-material systems − trends and innovations," Mechanics & Industry, vol. 24, p. 16, 2023, doi: 10.1051/meca/2023013.

[6] S. Wituschek, L. Elbel, and M. Lechner, "Versatile self-piercing riveting with a tumbling superimposed punch," Materials Research Proceedings, vol. 28, pp. 1111–1118, 2023, doi: 10.21741/9781644902479-122.

[7] P. Groche, D. Fritsche, E. A. Tekkaya, J. M. Allwood, G. Hirt, and R. Neugebauer, "Incremental Bulk Metal Forming," CIRP Annals, vol. 56, no. 2, pp. 635–656, 2007, doi: 10.1016/j.cirp.2007.10.006.

[8] S. Wituschek and M. Lechner, "Investigation of the influence of the tumbling angle on a tumbling self-piercing riveting process," Proceedings of the Institution of Mechanical Engineers, Part L: Journal of Materials: Design and Applications, vol. 236, no. 6, pp. 1302–1309, 2022, doi: 10.1177/14644207221080068.

[9] S. P. Sundar Singh Sivam, V. G. Uma Sekar, A. Mishra, A. Mondal, and S. Mishra, "Orbital Cold Forming Technology - Combining High Quality Forming with Cost Effectiveness - A Review," Indian Journal of Science and Technology, vol. 9, no. 38, 2016, doi: 10.17485/ijst/2016/v9i38/91426.

[10] M. M. Kasaei, R. Beygi, R. J. C. Carbas, E. A. S. Marques, and L. F. M. Da Silva, "A review on mechanical and metallurgical joining by plastic deformation," Discov Mechanical Engineering, vol. 2, no. 1, 2023, doi: 10.1007/s44245-023-00012-9.

[11] L. P. Troeger and E. A. Starke, "Microstructural and mechanical characterization of a superplastic 6xxx aluminum alloy," Materials Science and Engineering: A, vol. 277, 1-2, pp. 102–113, 2000, doi: 10.1016/S0921-5093(99)00543-2.

[12] DVS/EFB 3480-1 testing of properties of joints - testing of properties of mechanical and hybrid (mechanical/ bonded) joints., Deutscher Verband für Schweißen und verwandte Verfahren e.V. (DVS) / Europäische Forschungsgesellschaft Blech (EFB), Düsseldorf, 2007.

[13] S. Wituschek, "Combination of versatile self-piercing riveting processes," in Materials Research Proceedings, 2023, pp. 125–132, doi: 10.21741/9781644902417-16.